HHS Public Access

Author manuscript

Sci Transl Med. Author manuscript; available in PMC 2021 November 06.

Published in final edited form as:

Sci Transl Med. 2020 September 09; 12(560): . doi:10.1126/scitranslmed.aaz8631.

Therapeutic responses to *Roseomonas mucosa* in atopic dermatitis may involve lipid-mediated TNF-related epithelial repair

Ian A. Myles[1,2,*], **Carlo R. Castillo**[1,2], **Kent D. Barbian**[3], **Kishore Kanakabandi**[3], **Kimmo Virtaneva**[3], **Emily Fitzmeyer**[3], **Monica Paneru**[3], **Francisco Otaizo-Carrasquero**[4], **Timothy G. Myers**[4], **Tovah E. Markowitz**[5,6], **Ian N. Moore**[7], **Xue Liu**[8], **Marc Ferrer**[8], **Yosuke Sakamachi**[9], **Stavros Garantziotis**[9], **Muthulekha Swamydas**[10], **Michail S. Lionakis**[10], **Erik D. Anderson**[2], **Noah J. Earland**[2], **Sundar Ganesan**[11], **Ashleigh A. Sun**[2], **Jenna R.E. Bergerson**[2], **Robert A. Silverman**[12], **Maureen Petersen**[13], **Craig A. Martens**[3,†], **Sandip K. Datta**[2,†]

[1]Epithelial Therapeutics Unit, National Institute of Allergy and Infectious Disease, National Institutes of Health, Bethesda, MD, USA.

[2]Laboratory of Clinical Immunology and Microbiology, NIAID, NIH, Bethesda, MD, USA.

[3]RTS Genomics Unit, Rocky Mountain Laboratories, NIAID, NIH, Hamilton, MT, USA.

[4]Genomic Technologies Section, NIAID, NIH, Bethesda, MD, USA.

[5]NIAID Collaborative Bioinformatics Resource (NCBR), NIAID, NIH, Bethesda, MD, USA.

[6]Advanced Biomedical Computational Science, Frederick National Laboratory for Cancer Research, Frederick, MD, USA.

[7]Infectious Disease Pathogenesis Section, Comparative Medicine Branch, NIAID, NIH, Rockville, MD, USA.

[8]Department of Pre-clinical Innovation, National Center for Advancing Translational Sciences, NIH, Rockville, MD, USA.

[9]National Institute of Environmental Health Sciences, Research Triangle, NC, USA.

[*]Corresponding author. mylesi@niaid.nih.gov.

[†]These authors contributed equally to this work.

Author contributions: I.A.M. designed the study and experiments, evaluated patients, manufactured all treatment doses, and wrote the manuscript. C.R.C. assisted in select experiments involving epithelial cell culture and mouse sample collection, performed motility agar assessments, and assisted in patient sample collection. K.D.B. performed the bacterial transcriptomics analysis. K.K. and K.V. designed and validated isolate-specific qPCR primers. E.F. and M. Paneru assisted with bacterial RNA-seq experiments. F.O.-C. and T.G.M. performed RNA-seq on epithelial stem cells and analyzed the data. T.E.M. performed RNA-seq on fibroblasts, keratinocytes, and dendritic cells and analyzed the data. I.N.M. performed histological evaluations. X.L. and M.F. performed all trans-epidermal electrical resistance skin culture experiments. Y.S., S. Garantziotis, M.S., and M.S.L. provided genotyping, supplies, and intellectual input on mouse experiments involving TLR5 or CXCR2 knockout animals. E.D.A. and N.J.E. assisted in cellular scratch assay experiments. S. Ganesan assisted in analysis of all H&E-stained images. A.A.S. provided administrative assistance and performed blinded assessment of patients. J.R.E.B. helped to interpret experimental results. R.A.S. and M. Petersen provided clinical oversight for select patients. C.A.M. assisted in bacterial transcriptomics, provided data analysis for bacterial transcriptomics, helped to interpret experimental results, oversaw the project pertaining to bacterial assessments, and wrote the manuscript. S.K.D. provided intellectual expertise, helped to interpret experimental results, and wrote the manuscript.

SUPPLEMENTARY MATERIALS

stm.sciencemag.org/cgi/content/full/12/560/eaaz8631/DC1

Materials and Methods

[10]Fungal Pathogenesis Section, LCIM, NIAID, NIH, Bethesda, MD, USA.

[11]Biological Imaging Section, Research Technology Branch, NIAID, NIH, Bethesda, MD, USA.

[12]Department of Pediatrics, Georgetown University Hospital, Washington, DC, USA.

[13]Walter Reed National Military Medical Center, Bethesda, MD, USA.

Abstract

Dysbiosis of the skin microbiota is increasingly implicated as a contributor to the pathogenesis of atopic dermatitis (AD). We previously reported first-in-human safety and clinical activity results from topical application of the commensal skin bacterium *Roseomonas mucosa* for the treatment of AD in 10 adults and 5 children older than 9 years of age. Here, we examined the potential mechanism of action of *R. mucosa* treatment and its impact on children with AD less than 7 years of age, the most common age group for children with AD. In 15 children with AD, *R. mucosa* treatment was associated with amelioration of disease severity, improvement in epithelial barrier function, reduced *Staphylococcus aureus* burden on the skin, and a reduction in topical steroid requirements without severe adverse events. Our observed response rates to *R. mucosa* treatment were greater than those seen in historical placebo control groups in prior AD studies. Skin improvements and colonization by *R. mucosa* persisted for up to 8 months after cessation of treatment. Analyses of cellular scratch assays and the MC903 mouse model of AD suggested that production of sphingolipids by *R. mucosa*, cholinergic signaling, and flagellin expression may have contributed to therapeutic impact through induction of a TNFR2-mediated epithelial-to-mesenchymal transition. These results suggest that a randomized, placebo-controlled trial of *R. mucosa* treatment in individuals with AD is warranted and implicate commensals in the maintenance of the skin epithelial barrier.

INTRODUCTION

Atopic dermatitis (AD) is a common, allergic skin disease afflicting 5 to 25% of children worldwide (1). Although multifactorial in etiology, studies of AD pathogenesis increasingly implicate the commensal flora as a targetable contributor (2–5). The geographic distribution of AD rashes (6) overlaps with the distribution of cutaneous Gram-negative bacteria in healthy people (7) and individuals with AD have reduced carriage of Gram-negative bacteria (8). In addition to dysbiosis (an imbalance of microbes in or on the body), the skin of those with AD is deficient in sphingolipids (9, 10) and potential downstream antimicrobial peptides (11), even in the absence of clinical symptoms. The sphingolipid pathway, which includes sphingomyelins, ceramides, phospholipids, and arachidonic acid, has been directly linked to AD through its importance in the control of *Staphylococcus aureus*, epithelial barrier function, and immune regulation (9, 12, 13). On the basis of these reports, we hypothesized that defects in Gram-negative bacterial lipid production could contribute to AD. After modifying previous protocols for growing sphingolipid-producing bacteria (14), we reported a method for systematic collection of culturable Gram-negative bacteria (15). The most common species cultured from healthy volunteers was *Roseomonas mucosa* (3). Isolates of *R. mucosa* collected from healthy volunteers (*Rm*HV) improved outcomes in AD

murine and cell culture models (3). Isolates of *R. mucosa* collected from patients with AD (*Rm*AD) either had no effect or worsened outcomes in these models (3).

On the basis of these preclinical results, we initiated an open-label clinical trial and previously reported that topical treatment with live *Rm*HV in sucrose solution was safe and was associated with clinical improvement in 10 adult and 5 pediatric (ages 9 to 14) individuals with AD (2). However, both mechanism of action and therapeutic impact of *R. mucosa* treatment in young children with AD (under 7 years of age) remained unexplored. Here, we describe clinical assessment of an expanded cohort of children as young as 3 years of age with AD (expanded cohort, $n = 15$; total pediatric cohort $n = 20$; adult cohort, $n = 10$; tables S1 and S2). We provide mechanistic insights into *R. mucosa* activity associated with lipid-mediated activation of tumor necrosis factor receptor 2 (TNFR2)–related tissue repair pathways.

RESULTS

Clinical improvement in children with AD after *R. mucosa* treatment

Subsequent to the previously reported five patients with AD in our pediatric cohort (age 9 years or older) (2), we enrolled an additional 15 children with AD age 3 years or older (tables S1 and S2). Ten children with AD in this expanded pediatric cohort were treated with the previously described (2) dose escalation regimen of *R. mucosa* (Fig. 1A and fig. S1). The final five enrollees received a dose of 10^5 colony-forming units (CFU) per body site of *R. mucosa* for the entire 4 months of treatment (Fig. 1A and fig. S1). Patients or their guardians applied *R. mucosa* in sucrose directly to the antecubital and popliteal fossae as well as all other affected areas of the body. For both dosing strategies, *R. mucosa* treatment was associated with improvements in standard measures of severity, such as SCORing Atopic Dermatitis (SCORAD; mean improvement 64.3% for dose escalation and 69.4% for 10^5 CFU per body site; Fig. 1, B and C) and the Eczema Area and Severity Index (EASI; mean improvement 75.6% for dose escalation and 80.5% for 10^5 CFU per body site; Fig. 1, D and E). Most of the patients met both our primary and secondary endpoints at week 16: 85% (17 of 20) met our primary endpoint of a 50% reduction in SCORAD (SCORAD50; Table 1); 90% met the secondary endpoint of a 50% reduction in EASI (EASI50); 70% achieved EASI75, and 30% achieved EASI90 (Table 1). These response rates were greater than those seen in placebo control groups of prior AD studies (fig. S2A) (16–19) and were similar to response rates seen during open-label testing of the Food and Drug Administration–approved topical drugs tacrolimus and crisaborole (20, 21).

R. mucosa treatment response was similar for patients with AD classified as mild ($n = 11$; EASI <7) or moderate-severe ($n = 9$; EASI >7) upon enrollment (table S3). The improvements associated with *R. mucosa* treatment persisted for up to 8 months after treatment cessation. We observed residual mean improvements of 68.6 and 66.2% for SCORAD and 80.1 and 81.9% for EASI for the dose escalation and 10^5 CFU per body site cohorts, respectively (Fig. 1, B to E). *R. mucosa* treatment was associated with improvement on all actively treated body sites, including the antecubital and popliteal fossae (Fig. 1, F and G), the hands (Fig. 1H), neck (Fig. 1I), and trunk (Fig. 1J).

R. mucosa treatment was well tolerated and associated with improvements in AD-related features

R. mucosa treatment was associated with improvements in measurements related to AD. Epithelial barrier function improved in children with AD treated with *R. mucosa* as well as in cell culture models of epithelial physiology (Fig. 2A and fig. S2B). We observed a 14% mean reduction in trans-epidermal water loss (TEWL) in the skin of children with AD after treatment (Fig. 2A). We also observed improvements in trans-epidermal electrical resistance (a measure of epithelial barrier integrity) in full-thickness skin equivalents, an established skin epithelial model (22) comprising fibroblasts and keratinocytes that recapitulates the morphology and physiology of skin (fig. S2B). Treatment with *R. mucosa* was associated with additional improved measures: a 91.4% reduction in median and a 67.7% reduction in mean use of topical steroids (Fig. 2, B and C); a 60.5% reduction in pruritus (Fig. 2D); and improvement in the dermatology quality of life index for both the children (52%) and their families (58.4%; Fig. 2, E and F). As with the clinical measures, these improvements persisted for up to 8 months after cessation of *R. mucosa* treatment.

One report of self-limited pruritus at the application site was the only adverse event causally related to *R. mucosa* therapy (table S4). Treatment emergent events (reported at the time of treatment but not related to treatment) included two reports of viral upper respiratory infections, one diagnosis of hand, foot, and mouth disease coincident with a documented regional outbreak (23), and three mild AD flares after unintentional consumption of known food allergens (table S4).

R. mucosa treatment is associated with modest shifts in skin microbiota diversity

Similar to our prior reports (2), *R. mucosa* treatment was associated with a reduction in the culturable yield of *S. aureus* (mean reduction of 9.2×10^2 CFU/6.5cm^2 for dose escalation, 4.8×10^3 CFU/6.5cm^2 for the 10^5 CFU per body site dosing; 98.3% median reduction; $P = 0.08$) and a 98.7% reduction in the median ratio of *S. aureus* to coagulase-negative *Staphylococci* (Fig. 3A and fig. S2C; $P = 0.09$). However, prior failures of topical or oral antibiotics to provide lasting clinical benefit in AD (24) suggested that *S. aureus* reduction was unlikely to be the primary mechanism of benefit.

16*S* ribosomal RNA (rRNA) sequencing demonstrated that *R. mucosa* treatment was associated with modest changes in overall skin microbiota composition. This was indicated by the following: a reduction in the abundance of *Staphylococcaceae* (Fig. 3, B and C); an increase in the abundance of *Alphaproteobacteria*, the taxonomic class containing *R. mucosa* (Fig. 3, B and D); and an increase in the Shannon diversity index (Fig. 3E). Together, these changes suggested a shift toward a health-associated skin microbiota (8). Skin cultures suggested colonization with *R. mucosa* for up to 8 months after treatment (Fig. 3F). To assess whether *R. mucosa* cultured months after treatment cessation was due to colonization with therapeutic isolates, primers capable of identifying each of the three *Rm*HV treatment strains were derived. These primers demonstrated strain-specific polymerase chain reaction (PCR) signals that varied by treatment duration, body site, and dosing strategy (Fig. 3, G and H, and fig. S2, D and E). PCR signal strength did not correlate with clinical improvement (fig. S2, F and G); however, these primers were semiquantitative and may have been

influenced by differences in timing between skin sampling and previous *R. mucosa* dose. The amount of *R. mucosa* colonization indicated by PCR (Fig. 3, G and H) was similar to the culture yields from patients with AD after treatment (Fig. 3F) and healthy controls (25).

R. mucosa treatment is associated with alterations in TNF-related pathways

Serum cytokine measurements were consistent with anti-inflammatory outcomes (fig. S3), including reductions in tumor necrosis factor–α (TNFα) (fig. S3A) and interleukin-13 (IL-13) (fig. S3B). Changes in SCORAD were statistically associated with the percent change in TNFα concentrations as well as its downstream mediators (26, 27), hepatocyte growth factor (HGF) and IL-8 (CXCL8; Fig. 4A). Similar to prior reports (28), serum concentrations of thymus- and activation-regulated chemokine (TARC, CCL17) were also predictive of clinical response (Fig. 4A and fig. S3C; % change TARC/% change EASI = correlation 0.75; $P < 0.0001$). Additional mechanistic evaluations involved stimulation of primary cell monolayer cultures of human fibroblasts, hair follicle epithelial stem cells, keratinocytes, and dendritic cells with *Rm*HV, *Rm*AD, *S. aureus* isolated from individuals with AD, or coagulase-negative *Staphylococci* isolated from healthy volunteers. Focusing on the differential impact of *Rm*HV versus *Rm*AD across the different cell types, we found that *Rm*HV preferentially activated TNF and related downstream mediators: transforming growth factor–β (TGFβ), TNF superfamily 10 (TRAIL), and the HGF receptor c-Met (Fig. 4, B to E, and fig. S4, A to D). Pathway analysis suggested that these effects operated via the transcription factors nuclear factor κB (NFκB) and signal transducer and activator of transcription 3 (Stat3; Fig. 4E and fig. S4B). The predicted functional consequences of cell stimulation by *Rm*HV were activation of epithelial cell migration and proliferation related to an epithelial-to-mesenchymal transition (EMT; fig. S4, A and B). In contrast, coagulase-negative *Staphylococci* stimulation primarily affected protein metabolism pathways (fig. S4E). Top upstream regulators that distinguished coagulase-negative *Staphylococci* stimulation from *S. aureus* stimulation included type I interferon inhibition in fibroblasts and keratinocytes as well as *ERBB2* activation in dendritic cells (fig. S4F).

Reanalysis of published positive Genome Wide Association Studies (GWAS) associations with AD (29) indicated *STAT3* and *NFκB*-centric nodes linked by TNF and the TNF receptors, TNFR1 and TNFR2 (fig. S5A). However, unlike the serum cytokine data, *Rm*HV did not affect supernatant accumulation of TNFα in cultured epithelial cells, dendritic cells, or CD4/CD8 T cells (fig. S5B). Furthermore, TNF, TNFR1, and TNFR2 transcripts were not affected by *R. mucosa* treatment (Fig. 4, B to D).

R. mucosa activity in cellular and mouse models depends on TNFR2 signaling

The cellular scratch assay is an established functional assay for assessing tissue repair and EMT-mediated epithelial cell proliferation and migration (30, 31). In this assay, confluent cultures of epithelial cells are “scratched” with a sterile pipette tip (fig. S1). The resultant polarization induces epithelial cells to fill in the created space through NFκB-mediated (32) and STAT3-mediated (30) proliferation and migration governed by TGFβ (33). Incubation of cultured keratinocytes and fibroblasts with *Rm*HV but not *Rm*AD enhanced outcomes in these scratch assay cultures (Fig. 5, A to C). The addition of mitomycin C (an inhibitor

of cellular proliferation) reduced the efficacy of *Rm*HV in the cellular scratch assay for keratinocytes but not fibroblasts (fig. S5C). For both cell types, the effect of *Rm*HV was negated by blockade of TNFR2 and CXCR2 (IL-8R), but not TGFβR1 to TGFβR3 or c-Met (Fig. 5D).

Therapeutic responses to *R. mucosa* in the MC903 mouse model of chemically induced AD-like dermatitis (fig. S1) were also dependent on TNF-related pathways. The chemical MC903 was applied to mouse ears for 10 days, and then the animals received *R. mucosa* treatment or diluent control for 3 days after which mouse ear thickness, redness, and histology were scored. Diluent-treated control mice exhibited substantial epidermal hyperkeratosis and hyperplasia, as well as intracorneal cellular infiltrates that were consistent with serocellular crusting (inflammatory cells within thick keratin layers) and inflammatory expansion and infiltration of the underlying dermal stroma (Fig. 5, E and F). In wild-type mice, *Rm*HV treatment resulted in normalization of epidermal thickness and minimal cellular infiltration of the superficial keratin layer (stratum corneum) and the underlying dermis (Fig. 5, E and F). Furthermore, *Rm*HV treatment induced transcription of the EMT marker vimentin as well as the central EMT-regulator Snail1 (fig. S5D), both known to be directly modulated by TNFα (30, 34). In contrast to its effects in wild-type mice, *R. mucosa* treatment failed to improve outcomes in TNFR2-deficient mice, dual–TNF receptor–deficient mice (Fig. 5, E and F, and fig. S6A), or CXCR2-deficient mice (Fig. 5G and fig. S6B). Furthermore, *R. mucosa* treatment resulted in poorer outcomes in TNFR1-deficient mice and resulted in increased epidermal thickening or hyperplasia (Fig. 5, E and F), suggesting possible unchecked activation of TNFR2 or other mechanisms. MC903 mice deficient in NFκB (fig. S6, C to E) and mice with a transgenic insertion that mimics human STAT3 deficiency (a monogenic primary immune deficiency with an eczematous phenotype; mutant *Stat3*) demonstrated reduced inflammatory responses (fig. S6, F to H).

Glycerophospholipid production by *R. mucosa* influences TNFR2 signaling

To elucidate the microbial mechanisms responsible for the suggested induction of the TNF-IL8 signaling axis, we performed comparative transcriptomic (fig. S7A), differential metabolomic (Fig. 6A), and quantitative enzymatic (Fig. 6B) comparisons of three *Rm*HV and three *Rm*AD isolates (fig. S1). All three analyses identified differences in glycerophospholipid production between the *Rm*HV and *Rm*AD isolates. Consistent with reports demonstrating that glycerophospholipids influence EMT (35) and TNF signaling (26), crude lipid extracts from the *Rm*HV isolates improved cellular scratch assay outcomes in a TNFR2-dependent manner (Fig. 6C). Similarly, pretreatment of *Rm*HV with 1% lipase from *Candida* spp. negated therapeutic outcomes in the MC903 mouse model (Fig. 6D) without influencing bacterial growth kinetics (fig. S7B).

Glycerophospholipids that contain choline have been linked directly to AD by skin lipidomics (36) and indirectly through the clinical benefits of topical ceramides and coconut oil (10). In enzymatic assays, all *Rm*HV isolates trended toward greater acetylcholine content (Fig. 6E). Consistent with prior reports (37), cholinergic stimulation enhanced epithelial repair in the cellular scratch assay that was partially dependent on TNFR2 (Fig. 6F). Scratch assay activity of crude lipid extracts (Fig. 6G) or whole *Rm*HV isolates

(Fig. 6H) was reduced by pretreatment with mecamylamine, an antagonist of the nicotinic acetylcholine receptor (nAChR), but not atropine, an antimuscarinic drug. Furthermore, suspending *R. mucosa* in mecamylamine (Fig. 6, I and J) or genetic deletion of nAChRα7 (Fig. 6K) abolished the therapeutic effects of *R. mucosa* in our MC903 murine model of AD. The ability of 1% lipase to negate *Rm*HV activity (Fig. 6D) suggested that intact lipid residues may be required for a therapeutic effect, rather than the free choline liberated by lipase. Metabolomic analysis of antecubital tape strips collected from 14 patients before and after treatment with *R. mucosa* demonstrated an increase in sphingomyelin and related lipids (Fig. 6L and fig. S8) and suggested altered arachidonic acid metabolism in the skin after *R. mucosa* treatment (Fig. 6M).

In mice, direct links between the nAChR and serotonin have been described (38). Tryptophan metabolism differentiating *Rm*HV from *Rm*AD isolates (Fig. 6A) suggested possible additional neuromodulation of AD (39) and EMT via the serotonergic 5-HT_2 receptor (40). However, blockade of the 5-HT_2 receptor failed to affect our cellular scratch assay or MC903 mouse model (fig. S9, A and B) (41).

Potentiation of TNF activity by *R. mucosa* is influenced by Toll-like receptor 5

Lipid extracts from *Rm*HV enhanced epithelial coverage (Figs. 6C and 7A) but were unable to rescue deleterious effects of *Rm*AD in the cellular scratch assay (Fig. 7A). In addition, despite shared lipid profiles, one of the three treatment strains (designated *Rm*HV3) provided only partial benefit in the MC903 mouse model (Fig. 7B) and no benefit in the cellular scratch assay (Fig. 7C). To identify other potential mechanisms that may have modulated the beneficial effects of *Rm*HV treatment, we compared the transcriptional profiles of *Rm*HV1 and *Rm*HV2 with all other isolates. We found reduced expression of transcripts encoding proteins associated with the flagella or chemotaxis (Fig. 7D and fig. S10) in these beneficial *Rm*HV strains, which correlated with reduced bacterial migration in a functional motility assay (Fig. 7E).

Toll-like receptor 5 (TLR5), the innate receptor for the flagellar protein flagellin, was suppressed by *Rm*AD in fibroblasts (Fig. 4, C and D) and has been reported to influence allergic disease (42) as well as the induction of EMT by TNF (43). Consistent with a role for flagellin-TLR5 interactions, improved cellular scratch assay outcomes with *Rm*HV1 and *Rm*HV2 were abrogated by blockade of TLR5 (Fig. 7C) but not TLR2 or TLR4 (Fig. 7F). Recombinant flagellin demonstrated dose-dependent effects on cellular scratch assay outcomes that were TNFR2 dependent (Fig. 7, G and H). MC903-treated mice deficient in TLR5 (Fig. 7, I and J) or its downstream component MyD88 (Fig. 7K) did not respond to *R. mucosa* treatment. MC903-treated TLR4-deficient mice showed reduced ear thickness after *R. mucosa* treatment, and MC903-treated TLR2-deficient mice showed reduced disease severity (Fig. 7, I and J). The crude lipid fraction combined with recombinant flagellin and a synthetic cholinomimetic failed to provide benefit in MC903-treated mice (Fig. 7L), and coadministration of either 1% lipase or mecamylamine removed the residual benefit of *Rm*HV3 treatment (Fig. 7, M to O).

DISCUSSION

This early, open-label study was designed to evaluate whether the safety and activity of *R. mucosa* treatment could justify progression to a large, randomized, placebo-controlled clinical trial. In addition to encouraging safety and tolerability data, we found consistent patterns of improvement on several clinical measures in 15 children with AD treated with *R. mucosa*. We compared our results to data from historical cohorts cautiously. Our sucrose vehicle would not be expected to have placebo activity beyond the well-established rate of 10 to 30% (16–19), suggesting that our open-label results predict a favorable outcome in a future randomized, placebo-controlled, multisite trial.

Reports describing *R. mucosa* as an opportunistic pathobiont isolated from blood cultures and catheters (44) predated our discovery that *R. mucosa* could be a normal skin commensal capable of contaminating the cutaneous collection site (3, 15). Coisolation of *R. mucosa* with quintessential catheter pathogens like *S. aureus* in these studies additionally suggested a low virulence potential for *R. mucosa* given the recognized pathogenic potential of *S. aureus*. Safety claims for *R. mucosa* are further supported by the failure of *Rm*HV to generate notable pathology or infection after direct inoculation into the eyes, lungs, stomach, and veins of mice, in contrast to the morbidity and mortality seen with other skin commensals from healthy volunteers (3, 25). Thus, *R. mucosa* has yet to fulfill Koch's postulates for defining agents that cause infectious diseases. Instead, *R. mucosa* may fulfill the newly termed "commensal Koch's postulates" given that the strains used in this study have been associated with health, have been grown in pure culture, may ameliorate disease, and can be reisolated from treated patients (45).

Our mechanistic experiments suggested that the EMT known to contribute to epithelial homeostasis could be regulated by the microbiota present at epithelial surfaces and mediated by TNF signaling via IL-8, TLR5, and the nAChR (fig. S11). Our current results expand on our prior study that identified TNF-associated defects in EMT in patients with monogenic skin diseases due to STAT3 deficiency (30) and suggest a role for microbiota-mediated, TNF-induced EMT in common presentations of AD. These findings are also consistent with other studies showing sphingolipids associated with manifestations of AD including the following: direct suppression of *S. aureus* (9–11, 13, 36, 46); differential impact on allergic sensitization between TNFR1 and TNFR2 (47); atopic consequences associated with TLR5 activation (42); transcriptomic correlation between AD severity and keratinocyte differentiation (48); and EMT abnormalities underlying asthma, allergic rhinitis, and eosinophilic esophagitis (49). Our data are also consistent with reports showing that nAChR signaling influences AD, enhances skin barrier function, modulates TNF, and induces EMT (50–52). Failure of 5-HT_2 receptor blockade to affect our mouse or cell models (fig. S9, A and B) is consistent with reports that its modulation of TNF activity is limited to TNFR1 (41). Given that *S. aureus*–derived protein A directly activates TNFR1 (53), *R. mucosa* may also modulate TNF signaling through *S. aureus* suppression.

Although our findings suggest that activation of EMT-related pathways through bacterial lipids may be beneficial in the treatment of established AD, further work is needed to demonstrate that EMT is involved in AD pathogenesis. Whereas the current literature on

EMT understandably focuses on its role in neoplastic metastasis, it is an essential pathway for the renewal of epithelial tissues that are subjected to constant environmental insults. EMT has been associated with reduced barrier function in monolayer cultures of gingival cells (54). The effects of EMT on full-thickness epithelial tissue repair and differentiation may underlie *Rm*HV-associated enhancement of the epithelial barrier reported in mice (3), in full-thickness skin equivalents (fig. S2B), and in children with AD (Fig. 2A).

Our finding that a proinflammatory cytokine TNFα paradoxically may be beneficial in AD highlights the complexity of TNFα signaling. Most studies focus on soluble TNFα in serum, but TNF also exists in a membrane-bound form that can serve as both a signaling ligand for adjacent cells and a receptor for the cell expressing it (44). Neutralization of soluble TNFα can be anti-inflammatory when treating rheumatological diseases such as psoriasis, but loss of soluble TNFα through genetic deletion of ADAM17 (the enzyme that solubilizes membrane-bound TNFα) leads to spontaneous dysbiotic eczematous dermatitis in mice (5). TNF activity is also dependent on the signaling balance between TNFR1 and TNFR2. TNFR1 is central to the induction of cellular death pathways, whereas TNFR2 is a key mediator of EMT and cell proliferation (55). Both receptors are involved in antibacterial responses and inflammation (44). Results in our MC903 mouse model indicate that neither TNFR1 nor TNFR2 was required for chemically induced dermatitis, yet both receptors were required for therapeutic responses to *Rm*HV (Fig. 5, E and F). More recently, TNFR2 signaling was shown to be required for the proliferation, differentiation, and function of induced peripheral T regulatory cells (56). Furthermore, TNF-associated induction of EMT is cell type dependent and exhibits a hormetic dose-response curve (30). Our current results suggest that select TNF pathways are also dependent on costimulation of TLR5 and the nAChr.

Previous reports suggest that TARC could be a marker of improvement in AD and may connect TNF-mediated mechanisms with observed reductions in serum IL-13 (fig. S3, A to C) (28). Early reports suggested that TNF may induce TARC (57), but more recent studies suggest that the balance between TNFR1 and TNFR2 activation influences the impact of TNF signaling on TARC and IL-13 (58). Changes in serum cytokine concentrations in our study indicated that *R. mucosa* treatment exerted systemic effects (Fig. 4A and fig. S3), but the failure to affect serum IgE or eosinophilia (table S2) suggested that either *Rm*HV cannot reverse established atopy or that a longer treatment is required.

There are a number of limitations to our study. The primary limitation is the small, open-label design relying on historical placebo control data. Our mechanistic findings are limited by the muted inflammatory response to MC903-induced dermatitis observed in NFκB$^{-/-}$, mut*Stat3*, and TLR2$^{-/-}$ mice, which restricts assessment of the contribution of these specific pathways to *Rm*HV activity. Furthermore, we were unable to directly assess EMT pathways in the children with AD undergoing *R. mucosa* treatment because the invasive skin biopsies required would be unlikely to meet ethical guidelines for pediatric cohorts. However, our molecular annotations of the tape strips collected from children after *R. mucosa* treatment suggested that similar pathways to those identified in our MC903 mouse model were involved. Future mechanistic insights could be derived from metagenomic analysis of gut commensals, skin bacteria, and lipid-dependent skin fungi that are associated with allergic

disease (59–61). Insights could also come from evaluation of changes in peripheral and skin resident T cells, testing for *Rm*HV activity in additional mouse models of AD (62), and comparative genomics of *Rm*HV and *Rm*AD isolates. Furthermore, screening patients for genetic modifiers of AD such as filaggrin (63) may elucidate why some patients did not respond to treatment despite achieving colonization with *R. mucosa*.

Prior reports have established that adrenergic signaling inhibits EMT (64), chronic stress is a risk factor for atopy (65), and AD is associated with elevated catecholamine degradation (66). Thus, the differences in tyrosine metabolism between *Rm*HV and *Rm*AD isolates (Fig. 6A) as well as the change in tyrosine metabolism identified in the tape strips collected from children treated with *R. mucosa* (Fig. 6M) suggest a possible role for tyrosine-derived catecholamines in *Rm*HV activity. Potential reductions in catecholamines could modulate therapeutic responses by influencing the complex balance between optimal TLR5 activation by flagellin and nAChR activation by bacterial lipids in the potentiation of TNFR2 signaling (67). Each of these pathways may exert some protection as seen in our in vitro models, but the lipase sensitivity of the *R. mucosa* isolates tested in our MC903 mouse model suggests that a lipid-mediated mechanism requiring live *R. mucosa* colonization may be needed for therapeutic benefit. Screening other Gram-negative commensals, including additional *R. mucosa* strains from healthy volunteers, for similar metabolite profiles may help to elucidate other microbial mediators of *R. mucosa*'s beneficial effects.

Achieving clinical benefits from live biotherapeutic products may require changes to conventional drug development processes. The traditional expectations of dose-response data may not apply to live biotherapeutic products that can expand or contract to fit a biological niche and that may be subject to quorum-mediated effects. In addition, current pharmaceutical metabolite synthesis may be incompatible with some microbial physiology. Efficacy of extracted lipid metabolites from *Rm*HV might be enhanced by micelle optimization or chemical stabilizers, but intermittent topical lipid application may not be able to replicate the benefits of long-term colonization by *R. mucosa*. Our study, although limited by its small size and open-label design, suggests that a larger randomized, placebo-controlled clinical trial is warranted. Our findings also should prompt further investigation into the impact of microbes on EMT as well as potential TNF-associated deficits that may alter the skin microbiota.

MATERIALS AND METHODS

Study design

The objective of our mechanistic work in mice and in cellular scratch assays was to evaluate pathways through which *R. mucosa* from healthy volunteers (*Rm*HV) may provide benefit in the MC903 mouse model of AD. All murine experiments were done in compliance with the guidelines of the National Institute of Allergy and Infectious Disease (NIAID) Institutional Animal Care and Use Committee.

Our primary clinical objective was to assess the safety of topical treatment with *R. mucosa* in 21 children with AD age 3 years or older and to examine potential beneficial effects exceeding those reported in historical placebo control cohorts. The study was non-

randomized and open label. Patients were recruited and enrolled at the National Institutes of Health (NIH) under clinical trial no. NCT03018275 after approval from the NIAID institutional review board. All participants or their guardians provided informed consent before their participation in the study. For this study, 16 children with AD were enrolled (ages 3 to 17 years), 1 withdrew before treatment, and 15 were treated with live, topical *R. mucosa* twice weekly for 3 months, then every other day for an additional month, followed by a 4- to 12-month washout period. Assessments of clinical severity, epithelial barrier function, skin microbiota in the antecubital and popliteal fossae, and metabolomics analysis of tape strips from the antecubital fossae were performed.

Statistical comparisons were made against historical placebo controls achieving 30% or less on SCORAD50 as described previously (2). EASI scores were calculated as previously described (68). The study enrolled a total of 10 adults (patients 1.01 to 1.10) and 21 children (2.01 to 2.21). Patient 2.08 withdrew from the study before the week 4 visit and thus was not presented in any analysis. In this study, data for SCORAD, TEWL, pruritus, steroid use, family daily life quality index (FDLQI)/children daily life quality index (CDLQI), and the ratio of *S. aureus* to coagulase-negative *Staphylococci* included all pediatric participants that completed the study (2.01 to 2.07 and 2.09 to 2.21). All adult participant data and clinical data from patients 2.01 to 2.05 were presented previously (2). Adult participant data are presented in tables S3 and S4 for comparison only. All clinical data, with the addition of EASI, included all pediatric patients who completed the protocol. 16*S* rRNA and reverse transcription quantitative PCR (RTqPCR) analyses for specific *Rm*HV identification included all pediatric patients who completed the protocol. Tape strip data were collected from patients 2.07 and 2.09 to 2.21. Serum cytokines were assessed on frozen serum samples from weeks 0 and 16 using a multiplex kit per manufacturer's instructions (Bio-Rad).

Skin microbiota evaluation

16*S* bacterial microbiome assessment was performed by Admera Health (South Plainfield, NJ) as arranged through Science Exchange (Palo Alto, CA). For patients 2.01 to 2.05, genomic DNA was isolated using Qiagen QIAamp DNA mini kit per manufacturer's instructions (Qiagen, Hilden, Germany). Up to 15 ng of isolated genomic DNA was used to amplify via PCR with proprietary primers (Admera Health) covering hypervariable regions V3 and V4. Primer selection and design were chosen to achieve comprehensive taxonomic coverage, elimination of spike-in to gain maximal data. Data analysis was performed using Illumina 16S Metagenomics app, which performs taxonomic classification with the Greengenes database.

Metabolomics

Bacterial metabolomics were performed as previously described (2). Data were exported from Elements (Proteome Software, Portland, OR) into MetaboAnalyst (McGill University, Toronto, Canada) and uploaded under mass/charge ratio (m/z) to pathway analysis for *Pseudomonas*. Host metabolomics were performed by applying two sequential D-squame tape strips (Eurofins, Luxembourg) to the patient's antecubital fossa of the dominant hand. The second strip was taken from directly under the first to assess two layers. Samples

were frozen at −70°C until extracted with 900 μl of methanol and processed in an identical fashion as the bacterial metabolites. Raw-file *m*/*z* results were loaded into MetaboAnalyst *m*/*z* to pathway analysis. Annotations for metabolites deemed significantly different after versus before treatment under paired analysis annotated by METLIN (Scripps, La Jolla, CA), LIPID MAPS (lipidmaps.org), and MetaboAnalyst.

Cell culture studies

Primary human fibroblasts were a gift from M. Boehm (National Cancer Institute, Bethesda, MD). Primary human keratinocytes were collected and cultured as previously described (69). Ninety-six–well plate scratch cultures using fibroblasts were coated overnight with rat tail collagen (Roche, Basel, Switzerland) at 4°C. Dendritic cells were cultured and stimulated as previously described (70, 71). Human epithelial follicle stem cells were purchased from Celprogen (Torrance, CA) and cultured under manufacturer's recommendations. Epithelial stem cells were stimulated in an identical manner to fibroblast and keratinocyte cultures. Scratch assay for both keratinocytes and fibroblasts were performed as previously described (30) using a multiplicity of infection of 1 for all experiments.

Mouse studies

The MC903 model was performed as previously described (2) using 10^6 total CFU/ear of *R. mucosa*. Briefly, mice were treated with MC903 topically on each ear daily for 8 days. *R. mucosa* or metabolite treatment was applied daily for 3 days after MC903. Wild-type C57BL/6, Balbc/J, NFκB$^{-/-}$ (JAX06097), mutStat3 (JAX27952), TNFR1$^{-/-}$ (JAX3242), TNFR2$^{-/-}$ (JAX03246), TNFRdKO (JAX03243), TLR2$^{-/-}$ (JAX04650), CXCR2$^{-/-}$ (JAX02724), TLR5$^{-/-}$ (JAX28909), C3H (JAX00661), nAChRα7$^{-/-}$ (JAX03232), and MyD88$^{-/-}$ (JAX09088) were purchased from Jackson Laboratories (Bar Harbor, ME). Ear homogenization, RNA extraction, and quantitative PCR (qPCR) analysis were performed as previously described (30). For select experiments *R. mucosa* was suspended in Hanks' balanced salt solution (HBSS; Life Technologies, Grand Island, NY) containing a final concentration of 5 μM mecamylamine or atropine (Sigma-Aldrich), carbachol at a final concentration 1 μM, or 100 nM ketaserin (Sigma-Aldrich). Recombinant flagellin (FLA-BS Ultrapure; InvivoGen) was applied to mouse ears at a final concentration of 100 ng per ear in HBSS. When flagellin and/or carbachol were combined with *Rm*HV lipid fractions, final concentrations were maintained by diluting carbachol and/or flagellin into ethanol containing the lipid fraction for a final concentration of 80% ethanol. For select experiments, *R. mucosa* was cultured in R2A broth (Teknova, Hollister, CA) containing 1% lipase (v/v) from *Candida* spp. (Sigma-Aldrich). After pelleting, *R. mucosa* was suspended in HBSS and lipase was again added for a final concentration of 1% before application.

Statistical analysis

To determine statistical significance, unpaired *t* test, paired *t* test, Mann-Whitney *U* test, or one-way analysis of variance (ANOVA) with multiple-comparison corrections were applied using GraphPad Prism 8 software (San Diego, CA). Data are presented as the means ± SEM. A *P* value of less than 0.05 was considered significant.

Supplementary Material

Refer to Web version on PubMed Central for supplementary material.

Acknowledgments:

We thank the patients and their families. We thank B. Snow, K. Young, P. Welch, C. LaFeer, D. Darnell, and L. Barnhardt for administrative assistance (NIAID); the Center for Cancer Research Sequencing Facility (CCR-SF) for generating RNA-seq data; A. Saleem and M. Kieh (NIAID) for assistance in preparing the treatment doses; S. Hunsberger for statistical guidance; and R. Munford for help with lipid extraction. We also thank the NIAID building 33 veterinarians, animal care, and breeder technicians for assistance as well as Mr. and Mrs. Topolino (NIAID) for technical input on the murine studies.

Competing interests: S.K.D. is currently employed by Merck & Co Inc.; Merck did not provide funding or input to this project. X.L. is currently employed by L'Oreal USA; L'Oreal did not provide funding or input to this project. *R. mucosa* therapy has been patented by the NIH/NIAID and licensed through Forte Biosciences. I.A.M. and S.K.D. are coinventors on patent no. US 2019–10195236 entitled "Use of *R. mucosa* in the treatment of atopic dermatitis." Forte Biosciences did not provide funding or input to this project.

Funding:

This work was supported by the Intramural Research Program of NIAID and the NIH. Work related to trans-epidermal electrical resistance cell models was supported by the NIH Intramural Research Program as well as Cures Acceleration Network to NCATS.

Data and materials availability:

All data associated with this study are present in the paper or the Supplementary Materials. RNA-seq transcriptomics data for human cell cultures are available under the Gene Expression Omnibus (GEO) accession number GSE146184. Requests for materials should be directed to I.A.M. at mylesi@niaid.nih.gov and will be made available under a material transfer agreement.

REFERENCES AND NOTES

1. Morales E, Strachan D, Asher I, Ellwood P, Pearce N, Garcia-Marcos L; ISAAC phase III study group, Combined impact of healthy lifestyle factors on risk of asthma, rhinoconjunctivitis and eczema in school children: ISAAC phase III. Thorax 74, 531–538 (2019). [PubMed: 30898896]
2. Myles IA, Earland NJ, Anderson ED, Moore IN, Kieh MD, Williams KW, Saleem A, Fontecilla NM, Welch PA, Darnell DA, Barnhart LA, Sun AA, Uzel G, Datta SK, First-in-human topical microbiome transplantation with *Roseomonas mucosa* for atopic dermatitis. JCI Insight 3, e120608 (2018).
3. Myles IA, Williams KW, Reckhow JD, Jammeh ML, Pincus NB, Sastalla I, Saleem D, Stone KD, Datta SK, Transplantation of human skin microbiota in models of atopic dermatitis. JCI Insight 1, e86955 (2016).
4. Nakatsuji T, Chen TH, Narala S, Chun KA, Two AM, Yun T, Shafiq F, Kotol PF, Bouslimani A, Melnik AV, Latif H, Kim J-N, Lockhart A, Artis K, David G, Taylor P, Streib J, Dorrestein PC, Grier A, Gill SR, Zengler K, Hata TR, Leung DY, Gallo RL, Antimicrobials from human skin commensal bacteria protect against Staphylococcus aureus and are deficient in atopic dermatitis. Sci. Transl. Med 9, eaah4680 (2017). [PubMed: 28228596]
5. Kobayashi T, Glatz M, Horiuchi K, Kawasaki H, Akiyama H, Kaplan DH, Kong HH, Amagai M, Nagao K, Dysbiosis and Staphylococcus aureus colonization drives inflammation in atopic dermatitis. Immunity 42, 756–766 (2015). [PubMed: 25902485]
6. Sabin BR, Peters N, Peters AT, Chapter 20: Atopic dermatitis. Allergy Asthma Proc. 33 (Suppl 1), 67–69 (2012). [PubMed: 22794693]

7. Grice EA, Segre JA, The skin microbiome. Nat. Rev. Microbiol 9, 244–253 (2011). [PubMed: 21407241]
8. Kong HH, Oh J, Deming C, Conlan S, Grice EA, Beatson MA, Nomicos E, Polley EC, Komarow HD; NISC Comparative Sequence Program, Murray PR, Turner ML, Segre JA, Temporal shifts in the skin microbiome associated with disease flares and treatment in children with atopic dermatitis. Genome Res. 22, 850–859 (2012). [PubMed: 22310478]
9. Arikawa J, Ishibashi M, Kawashima M, Takagi Y, Ichikawa Y, Imokawa G, Decreased levels of sphingosine, a natural antimicrobial agent, may be associated with vulnerability of the stratum corneum from patients with atopic dermatitis to colonization by *Staphylococcus aureus*. J. Invest. Dermatol 119, 433–439 (2002). [PubMed: 12190867]
10. Bhattacharya N, Sato WJ, Kelly A, Ganguli-Indra G, Indra AK, Epidermal lipids: Key mediators of atopic dermatitis pathogenesis. Trends Mol. Med 25, 551–562 (2019). [PubMed: 31054869]
11. Park K, Lee S, Lee Y-M, Sphingolipids and antimicrobial peptides: Function and roles in atopic dermatitis. Biomol. Ther 21, 251–257 (2013).
12. Li Q, Fang H, Dang E, Wang G, The role of ceramides in skin homeostasis and inflammatory skin diseases. J. Dermatol. Sci 97, 2–8 (2019). [PubMed: 31866207]
13. Li S, Villarreal M, Stewart S, Choi J, Ganguli-Indra G, Babineau DC, Philpot C, David G, Yoshida T, Boguniewicz M, Hanifin JM, Beck LA, Leung DY, Simpson EL, Indra AK, Altered composition of epidermal lipids correlates with *Staphylococcus aureus* colonization status in atopic dermatitis. Br. J. Dermatol 177, e125–e127 (2017). [PubMed: 28244066]
14. Vaz-Moreira I, Nunes OC, Manaia CM, Diversity and antibiotic resistance patterns of *Sphingomonadaceae* isolates from drinking water. Appl. Environ. Microbiol 77, 5697–5706 (2011). [PubMed: 21705522]
15. Myles IA, Reckhow JD, Williams KW, Sastalla I, Frank KM, Datta SK, A method for culturing Gram-negative skin microbiota. BMC Microbiol. 16, 60 (2016). [PubMed: 27052736]
16. Snast I, Reiter O, Hodak E, Friedland R, Mimouni D, Leshem YA, Are biologics efficacious in atopic dermatitis? A systematic review and meta-analysis. Am. J. Clin. Dermatol 19, 145–165 (2018). [PubMed: 29098604]
17. Alexis AF, Rendon M, Silverberg JI, Pariser DM, Lockshin B, Griffiths CE, Weisman J, Wollenberg A, Chen Z, Davis JD, Li M, Eckert L, Gadkari A, Shumel B, Rossi AB, Graham NM, Ardeleanu M, Efficacy of dupilumab in different racial subgroups of adults with moderate-to-severe atopic dermatitis in three randomized, placebo-controlled phase 3 trials. J. Drugs Dermatol 18, 804–813 (2019). [PubMed: 31424712]
18. Lee J, Seto D, Bielory L, Meta-analysis of clinical trials of probiotics for prevention and treatment of pediatric atopic dermatitis. J. Allergy Clin. Immunol 121, 116–121.e11 (2008). [PubMed: 18206506]
19. Fishbein AB, Mueller K, Lor J, Smith P, Paller AS, Kaat A, Systematic review and meta-analysis comparing topical corticosteroids with vehicle/moisturizer in childhood atopic dermatitis. J. Pediatr. Nurs 47, 36–43 (2019). [PubMed: 31026679]
20. Tom WL, Van Syoc M, Chanda S, Zane LT, Pharmacokinetic profile, safety, and tolerability of crisaborole topical ointment, 2% in adolescents with atopic dermatitis: An open-label phase 2a study. Pediatr. Dermatol 33, 150–159 (2016). [PubMed: 26777394]
21. Mandelin JM, Rubins A, Remitz A, Cirule K, Dickinson J, Ho V, Mäkelä MJ, Rubins S, Reitamo S, Undre N, Long-term efficacy and tolerability of tacrolimus 0.03% ointment in infants:* A two-year open-label study. Int. J. Dermatol 51, 104–110 (2012). [PubMed: 21923693]
22. Liu X, Michael S, Bharti K, Ferrer M, Song MJ, A biofabricated vascularized skin model of atopic dermatitis for preclinical studies. Biofabrication 12, 035002 (2020). [PubMed: 32059197]
23. Larche J, WTKR CBS News (2018); https://wtkr.com/2018/07/31/morning-rounds-hand-foot-and-mouth-disease/.
24. Eichenfield LF, Ahluwalia J, Waldman A, Borok J, Udkoff J, Boguniewicz M, Current guidelines for the evaluation and management of atopic dermatitis: A comparison of the Joint Task Force Practice Parameter and American Academy of Dermatology guidelines. J. Allergy Clin. Immunol 139, S49–S57 (2017). [PubMed: 28390477]

25. Myles IA, Moore IN, Castillo CR, Datta SK, Differing virulence of healthy skin commensals in mouse models of infection. Front. Cell. Infect. Microbiol 8, 451 (2019). [PubMed: 30719426]
26. Treede I, Braun A, Jeliaskova P, Giese T, Füllekrug J, Griffiths G, Stremmel W, Ehehalt R, TNF-α-induced up-regulation of pro-inflammatory cytokines is reduced by phosphatidylcholine in intestinal epithelial cells. BMC Gastroenterol. 9, 53 (2009). [PubMed: 19594939]
27. Bigatto V, De Bacco F, Casanova E, Reato G, Lanzetti L, Isella C, Sarotto I, Comoglio PM, Boccaccio C, TNF-α promotes invasive growth through the MET signaling pathway. Mol. Oncol 9, 377–388 (2015X). [PubMed: 25306394]
28. Beck LA, Thaci D, Hamilton JD, Graham NM, Bieber T, Rocklin R, Ming JE, Ren H, Kao R, Simpson E, Ardeleanu M, Weinstein SP, Pirozzi G, Guttman-Yassky E, Suarez-Farinas M, Hager MD, Stahl N, Yancopoulos GD, Radin AR, Dupilumab treatment in adults with moderate-to-severe atopic dermatitis. N. Engl. J. Med 371, 130–139 (2014). [PubMed: 25006719]
29. Bin L, Leung DY, Genetic and epigenetic studies of atopic dermatitis. Allergy Asthma Clin. Immunol 12, 52 (2016). [PubMed: 27777593]
30. Myles IA, Anderson ED, Earland NJ, Zarember KA, Sastalla I, Williams KW, Gough P, Moore IN, Ganesan S, Fowler CJ, Laurence A, Garofalo M, Kuhns DB, Kieh MD, Saleem A, Welch PA, Darnell DA, Gallin JI, Freeman AF, Holland SM, Datta SK, TNF overproduction impairs epithelial staphylococcal response in hyper IgE syndrome. J. Clin. Invest 128, 3595–3604 (2018). [PubMed: 30035749]
31. Nieto MA, Huang RY-J, Jackson RA, Thiery JP, Emt: 2016. Cell 166, 21–45 (2016). [PubMed: 27368099]
32. Park YR, Sultan MT, Park HJ, Lee JM, Ju HW, Lee OJ, Lee DJ, Kaplan DL, Park CH, NF-κB signaling is key in the wound healing processes of silk fibroin. Acta Biomater. 67, 183–195 (2018). [PubMed: 29242162]
33. Xu J, Lamouille S, Derynck R, TGF-β-induced epithelial to mesenchymal transition. Cell Res. 19, 156–172 (2009). [PubMed: 19153598]
34. Wu Y, Zhou BP, TNF-α/NF-κB/Snail pathway in cancer cell migration and invasion. Br. J. Cancer 102, 639–644 (2010). [PubMed: 20087353]
35. Sampaio JL, Gerl MJ, Klose C, Ejsing CS, Beug H, Simons K, Shevchenko A, Membrane lipidome of an epithelial cell line. Proc. Natl. Acad. Sci. U.S.A 108, 1903–1907 (2011). [PubMed: 21245337]
36. Berdyshev E, Goleva E, Bronova I, Dyjack N, Rios C, Jung J, Taylor P, Jeong M, Hall CF, Richers BN, Norquest KA, Zheng T, Seibold MA, Leung DY, Lipid abnormalities in atopic skin are driven by type 2 cytokines. JCI Insight 3, e98006 (2018).
37. Lu J-J, Xu G-N, Yu P, Song Y, Wang X-L, Zhu L, Chen H-Z, Cui Y-Y, The activation of M3 mAChR in airway epithelial cells promotes IL-8 and TGF-β1 secretion and airway smooth muscle cell migration. Respir. Res 17, 25 (2016). [PubMed: 26956674]
38. Levin ED, Slade S, Johnson M, Petro A, Horton K, Williams P, Rezvani AH, Rose JE, Ketanserin, a 5-HT_2 receptor antagonist, decreases nicotine self-administration in rats. Eur. J. Pharmacol 600, 93–97 (2008). [PubMed: 18950618]
39. Lonne-Rahm SB, Rickberg H, El-Nour H, Mårin P, Azmitia EC, Nordlind K, Neuroimmune mechanisms in patients with atopic dermatitis during chronic stress. J. Eur. Acad. Dermatol. Venereol 22, 11–18 (2008). [PubMed: 18181968]
40. Sadiq A, Shah A, Jeschke MG, Belo C, Qasim Hayat M, Murad S, Amini-Nik S, The role of serotonin during skin healing in post-thermal injury. Int. J. Mol. Sci 19, 1034 (2018).
41. Pelletier M, Siegel RM, Wishing away inflammation? New links between serotonin and TNF signaling. Mol. Interv 9, 299–301 (2009). [PubMed: 20048135]
42. Prescott SL, Noakes P, Chow BW, Breckler L, Thornton CA, Hollams EM, Ali M, van den Biggelaar AH, Tulic MK, Presymptomatic differences in Toll-like receptor function in infants who have allergy. J. Allergy Clin. Immunol 122, 391–399.e5 (2008). [PubMed: 18571707]
43. Thagia I, Shaw EJ, Smith E, Else KJ, Rigby RJ, Intestinal epithelial suppressor of cytokine signaling 3 enhances microbial-induced inflammatory tumor necrosis factor-α, contributing to epithelial barrier dysfunction. Am. J. Physiol. Gastrointest. Liver Physiol 308, G25–G31 (2015). [PubMed: 25377316]

44. Sedger LM, McDermott MF, TNF and TNF-receptors: From mediators of cell death and inflammation to therapeutic giants – past, present and future. Cytokine Growth Factor Rev. 25, 453–472 (2014). [PubMed: 25169849]
45. Neville BA, Forster SC, Lawley TD, Commensal Koch's postulates: Establishing causation in human microbiota research. Curr. Opin. Microbiol 42, 47–52 (2018). [PubMed: 29112885]
46. Elias PM, Lipid abnormalities and lipid-based repair strategies in atopic dermatitis. Biochim. Biophys. Acta 1841, 323–330 (2014). [PubMed: 24128970]
47. Whitehead GS, Thomas SY, Shalaby KH, Nakano K, Moran TP, Ward JM, Flake GP, Nakano H, Cook DN, TNF is required for TLR ligand-mediated but not protease-mediated allergic airway inflammation. J. Clin. Invest 127, 3313–3326 (2017). [PubMed: 28758900]
48. Ghosh D, Ding L, Sivaprasad U, Geh E, Biagini Myers J, Bernstein JA, Khurana Hershey GK, Mersha TB, Multiple transcriptome data analysis reveals biologically relevant atopic dermatitis signature genes and pathways. PLOS ONE 10, e0144316 (2015). [PubMed: 26717000]
49. Schleimer RP, Berdnikovs S, Etiology of epithelial barrier dysfunction in patients with type 2 inflammatory diseases. J. Allergy Clin. Immunol 139, 1752–1761 (2017). [PubMed: 28583447]
50. Chen P-C, Lee W-Y, Ling H-H, Cheng C-H, Chen K-C, Lin C-W, Activation of fibroblasts by nicotine promotes the epithelial-mesenchymal transition and motility of breast cancer cells. J. Cell. Physiol 233, 4972–4980 (2018). [PubMed: 29215705]
51. Curtis BJ, Radek KA, Cholinergic regulation of keratinocyte innate immunity and permeability barrier integrity: New perspectives in epidermal immunity and disease. J. Invest. Dermatol 132, 28–42 (2012). [PubMed: 21918536]
52. Fujii T, Mashimo M, Moriwaki Y, Misawa H, Ono S, Horiguchi K, Kawashima K, Expression and function of the cholinergic system in immune cells. Front. Immunol 8, 1085 (2017). [PubMed: 28932225]
53. Gómez MI, Lee A, Reddy B, Muir A, Soong G, Pitt A, Cheung A, Prince A, *Staphylococcus aureus* protein A induces airway epithelial inflammatory responses by activating TNFR1. Nat. Med 10, 842–848 (2004). [PubMed: 15247912]
54. Sume SS, Kantarci A, Lee A, Hasturk H, Trackman PC, Epithelial to mesenchymal transition in gingival overgrowth. Am. J. Pathol 177, 208–218 (2010). [PubMed: 20489142]
55. Markopoulos GS, Roupakia E, Marcu KB, Kolettas E, Epigenetic regulation of inflammatory cytokine-induced epithelial-to-mesenchymal cell transition and cancer stem cell generation. Cell 8, 1143 (2019).
56. Yang S, Xie C, Chen Y, Wang J, Chen X, Lu Z, June RR, Zheng SG, Differential roles of TNFα-TNFR1 and TNFα-TNFR2 in the differentiation and function of $CD4^{+}Foxp3^{+}$ induced Treg cells in vitro and in vivo periphery in autoimmune diseases. Cell Death Dis. 10, 27 (2019). [PubMed: 30631042]
57. Xiao T, Fujita H, Saeki H, Mitsui H, Sugaya M, Tada Y, Kakinuma T, Torii H, Nakamura K, Asahina A, Tamaki K, Thymus and activation-regulated chemokine (TARC/CCL17) produced by mouse epidermal Langerhans cells is upregulated by TNF-α and IL-4 and downregulated by IFN-γ. Cytokine 23, 126–132 (2003). [PubMed: 12967648]
58. Kratochvill F, Neale G, Haverkamp JM, Van de Velde L-A, Smith AM, Kawauchi D, McEvoy J, Roussel MF, Dyer MA, Qualls JE, Murray PJ, TNF counterbalances the emergence of M2 tumor macrophages. Cell Rep. 12, 1902–1914 (2015). [PubMed: 26365184]
59. Han SH, Cheon HI, Hur MS, Kim MJ, Jung WH, Lee YW, Choe YB, Ahn KJ, Analysis of the skin mycobiome in adult patients with atopic dermatitis. Exp. Dermatol 27, 366–373 (2018). [PubMed: 29356103]
60. Jo J-H, Kennedy EA, Kong HH, Topographical and physiological differences of the skin mycobiome in health and disease. Virulence 8, 324–333 (2017). [PubMed: 27754756]
61. Lee SY, Lee E, Park YM, Hong SJ, Microbiome in the gut-skin axis in atopic dermatitis. Allergy Asthma Immunol. Res 10, 354–362 (2018). [PubMed: 29949831]
62. Jin H, He R, Oyoshi M, Geha RS, Animal models of atopic dermatitis. J. Invest. Dermatol 129, 31–40 (2009). [PubMed: 19078986]
63. Drislane C, Irvine AD, The role of filaggrin in atopic dermatitis and allergic disease. Ann. Allergy Asthma Immunol 124, 36–43 (2020). [PubMed: 31622670]

64. Pullar CE, Rizzo A, Isseroff RR, β-Adrenergic receptor antagonists accelerate skin wound healing: Evidence for a catecholamine synthesis network in the epidermis. J. Biol. Chem 281, 21225–21235 (2006). [PubMed: 16714291]
65. Barnthouse M, Jones BL, The impact of environmental chronic and toxic stress on asthma. Clin. Rev. Allergy Immunol 57, 427–438 (2019). [PubMed: 31079340]
66. Sivamani RK, Lam ST, Isseroff RR, Beta adrenergic receptors in keratinocytes. Dermatol. Clin 25, 643–653 (2007). [PubMed: 17903623]
67. Uchida M, Oyanagi E, Kawanishi N, Iemitsu M, Miyachi M, Kremenik MJ, Onodera S, Yano H, Exhaustive exercise increases the TNF-α production in response to flagellin via the upregulation of toll-like receptor 5 in the large intestine in mice. Immunol. Lett 158, 151–158 (2014). [PubMed: 24412598]
68. Hanifin JM, Thurston M, Omoto M, Cherill R, Tofte SJ, Graeber M; EASI Evaluator Group, The eczema area and severity index (EASI): Assessment of reliability in atopic dermatitis. Exp. Dermatol 10, 11–18 (2001). [PubMed: 11168575]
69. Anderson ED, Sastalla I, Earland NJ, Mahnaz M, Moore IN, Otaizo-Carrasquero F, Myers TG, Myles CA, Datta SK, Myles IA, Prolonging culture of primary human keratinocytes isolated from suction blisters with the Rho kinase inhibitor Y-27632. PLOS ONE 13, e0198862 (2018). [PubMed: 30208113]
70. Kieh MD, Datta SK, Myles IA, $CD8^+$ T cell dialyzable extract activity is dependent on TCR and MHC-I. J. Leukoc. Biol 102, 566–567 (2017). [PubMed: 28860203]
71. Myles IA, Zhao M, Nardone G, Olano LR, Reckhow JD, Saleem D, Break TJ, Lionakis MS, Myers TG, Gardina PJ, Kirkpatrick CH, Holland SM, Datta SK, $CD8^+$ T cells produce a dialyzable antigen-specific activator of dendritic cells. J. Leukoc. Biol 101, 307–320 (2017). [PubMed: 27515950]
72. Anders S, Pyl PT, Huber W, HTSeq—A Python framework to work with high-throughput sequencing data. Bioinformatics 31, 166–169 (2015). [PubMed: 25260700]
73. Dobin A, Davis CA, Schlesinger F, Drenkow J, Zaleski C, Jha S, Batut P, Chaisson M, Gingeras TR, STAR: Ultrafast universal RNA-seq aligner. Bioinformatics 29, 15–21 (2013). [PubMed: 23104886]
74. Langmead B, Salzberg SL, Fast gapped-read alignment with Bowtie 2. Nat. Methods 9, 357–359 (2012). [PubMed: 22388286]
75. Love MI, Huber W, Anders S, Moderated estimation of fold change and dispersion for RNA-seq data with DESeq2. Genome Biol. 15, 550 (2014). [PubMed: 25516281]
76. Martín A, Boisgard R, Kassiou M, Dollé F, Tavitian B, Reduced PBR/TSPO expression after minocycline treatment in a rat model of focal cerebral ischemia: A PET study using [18F]DPA-714. Mol. Imaging Biol 13, 10–15 (2011). [PubMed: 20383592]
77. Ritchie ME, Phipson B, Wu D, Hu Y, Law CW, Shi W, Smyth GK, *limma* powers differential expression analyses for RNA-sequencing and microarray studies. Nucleic Acids Res. 43, e47 (2015). [PubMed: 25605792]
78. Smits JPH, Niehues H, Rikken G, van Vlijmen-Willems I, van de Zande G, Zeeuwen P, Schalkwijk J, van den Bogaard EH, Immortalized N/TERT keratinocytes as an alternative cell source in 3D human epidermal models. Sci. Rep 7, 11838 (2017). [PubMed: 28928444]
79. Sriram G, Alberti M, Dancik Y, Wu B, Wu R, Feng Z, Ramasamy S, Bigliardi PL, Bigliardi-Qi M, Wang Z, Full-thickness human skin-on-chip with enhanced epidermal morphogenesis and barrier function. Mater. Today 21, 326–340 (2018).
80. Zhu F, Zhang Z, Wu G, Li Z, Zhang R, Ren J, Nong L, Rho kinase inhibitor fasudil suppresses migration and invasion though down-regulating the expression of VEGF in lung cancer cell line A549. Med. Oncol 28, 565–571 (2011). [PubMed: 20300976]

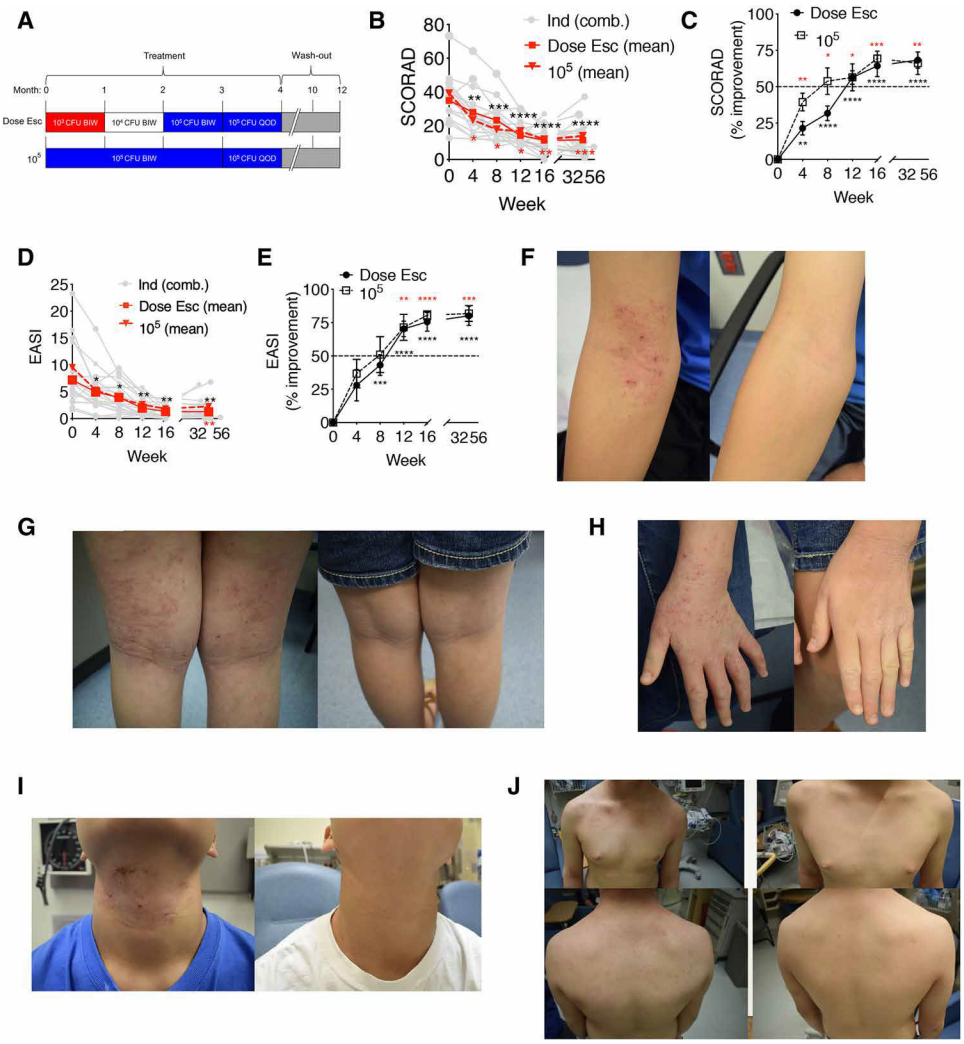

Fig. 1. Topical *R. mucosa* treatment is associated with clinical improvement.

(**A**) Summary of dosing strategy for *R. mucosa* including dose escalation (Dose Esc) and the maximum dose of 10^5 colony-forming units (CFU) per body site. BIW, twice weekly; QOD, every other day. (**B**) Mean SCORAD values (red solid line represents Dose Esc, $n = 15$; red dashed line represents 10^5 CFU/body site dose, $n = 5$) and individual SCORAD values (Ind, gray lines; $n = 20$) for patients with AD treated with *R. mucosa*. (**C**) % improvement (means ± SEM) on the SCORAD scale during *R. mucosa* treatment. (**D**) Mean EASI values (red solid line represents Dose Esc, $n = 15$; red dashed line represents 10^5 CFU/body site dose, $n = 5$) and individual EASI values (Ind, gray lines; $n = 20$) for patients with AD treated with *R. mucosa*. (**E**) % improvement (means ± SEM) on the EASI scale during *R. mucosa* treatment. (B to E) Black asterisks indicate dose escalation cohort, and red asterisks indicate 10^5 CFU/body site dose. *Y*-axis dashed line (C and E) indicates improvements inconsistent with the null hypothesis and primary endpoint target. (**F** to **I**) Representative photographs of body sites for study participants with AD at enrollment (week 0, left) and after 16 weeks of *R. mucosa* treatment (right) for the antecubital fossa (F), popliteal fossa (G), hands (H),

neck (I), and trunk (**J**). *$P < 0.05$, **$P < 0.01$, ***$P < 0.001$, and ****$P < 0.0001$ versus enrollment value by paired ANOVA with Dunnett correction.

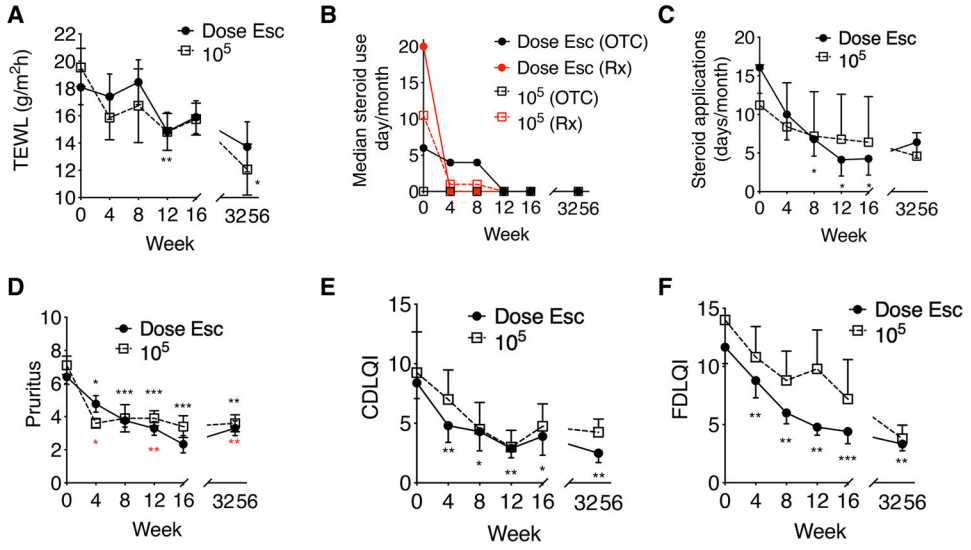

Fig. 2. Topical *R. mucosa* treatment is associated with improvements in AD.

(**A**) Mean values for trans-epidermal water loss (TEWL) during *R. mucosa* treatment and washout phase. (**B** and **C**) Median steroid cream applications per month for (B) over the counter (OTC) and prescription (Rx) topical steroid treatments and (C) mean values for combined steroid treatments [$n = 16$ for both (B) and (C)]. All topical steroid usage was reported as stable for months to years before enrollment of all patients with AD. Week 0 steroid usage reflects reported average steroid use over the 4 months before study enrollment. (**D**) Mean pruritus scores and (**E** and **F**) quality of life indices for study participants with AD treated with *R. mucosa*. (E and F) Children daily life quality index (CDLQI) (E) and (F) family daily life quality index (FDLQI); higher numbers indicate greater burden. Black asterisks are for dose escalation cohort, and red asterisks are for 10^5 CFU/body site dose. $*P < 0.05$, $**P < 0.01$, $***P < 0.001$ versus enrollment value by paired ANOVA with Dunnett correction.

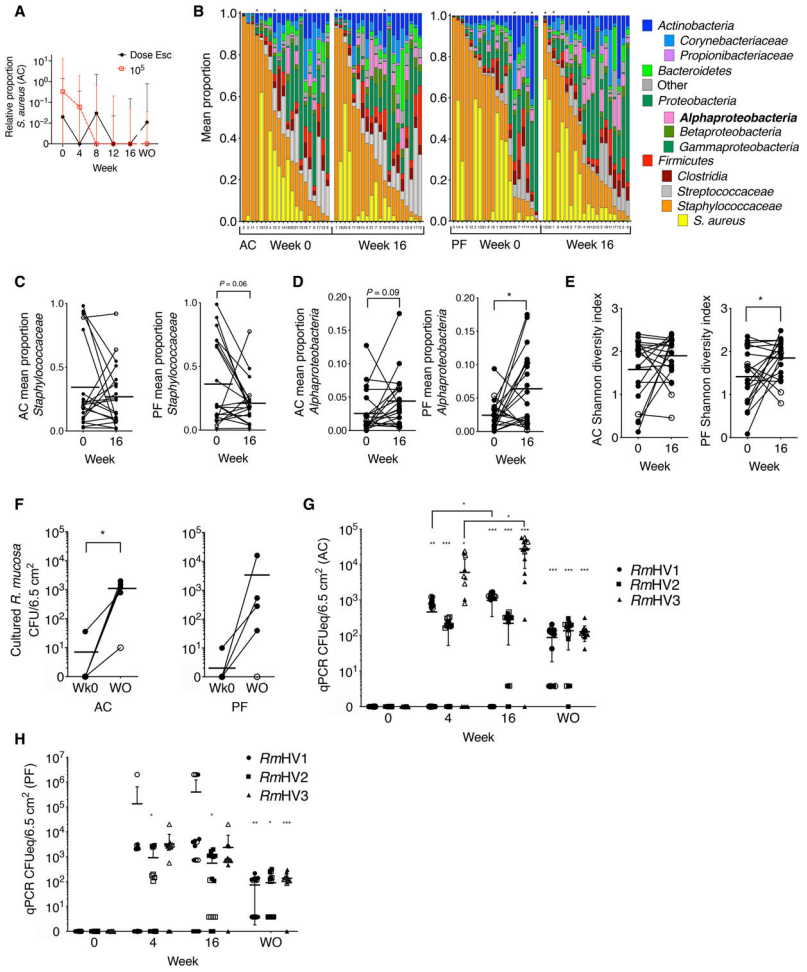

Fig. 3. Topical *R. mucosa* treatment is associated with long-term skin colonization.

(**A**) Shown are median ± interquartile range for relative abundance of *S. aureus* versus coagulase-negative *Staphylococci* in the antecubital fossa (AC) of patients with AD treated with *R. mucosa* at escalating doses (Dose Esc) or a 105 CFU/body site dose. (**B**) 16*S* rRNA sequencing of the skin microbiome in swabs from AC and popliteal fossa (PF) on weeks 0 and 16 of dose escalation. Columns are labeled by patient enrollment number but sorted by relative abundance of total *Staphylococcaceae*; black asterisks indicate patients who did not respond to *R. mucosa* treatment. (**C** to **E**) Relative proportions of indicated taxa (C and D) and Shannon diversity index (E) calculated from rRNA sequencing data in (B) for skin swabs from the AC and PF fossae; open circles represent nonresponding patients. (**F**) Culture-based enumeration of *R. mucosa* from antecubital and popliteal fossae (AC and PF) for the first five pediatric patients treated with *R. mucosa* at week 0 (Wk0) and at the washout visit (WO); open circles represent nonresponding patients. (**G** and **H**) Colony-forming unit equivalents (CFUeq) of *R. mucosa* from healthy volunteers (*Rm*HV) measured by RTqPCR from skin swabs from AC (G) and PF (H) body sites ($n = 15$ each) are shown. Closed symbols represent the dose escalation cohort; open symbols represent the 105 CFU/body site dose cohort. *$P < 0.05$, **$P < 0.01$, and ***$P < 0.001$ by paired ANOVA with Dunnett correction versus week 0 value unless indicated.

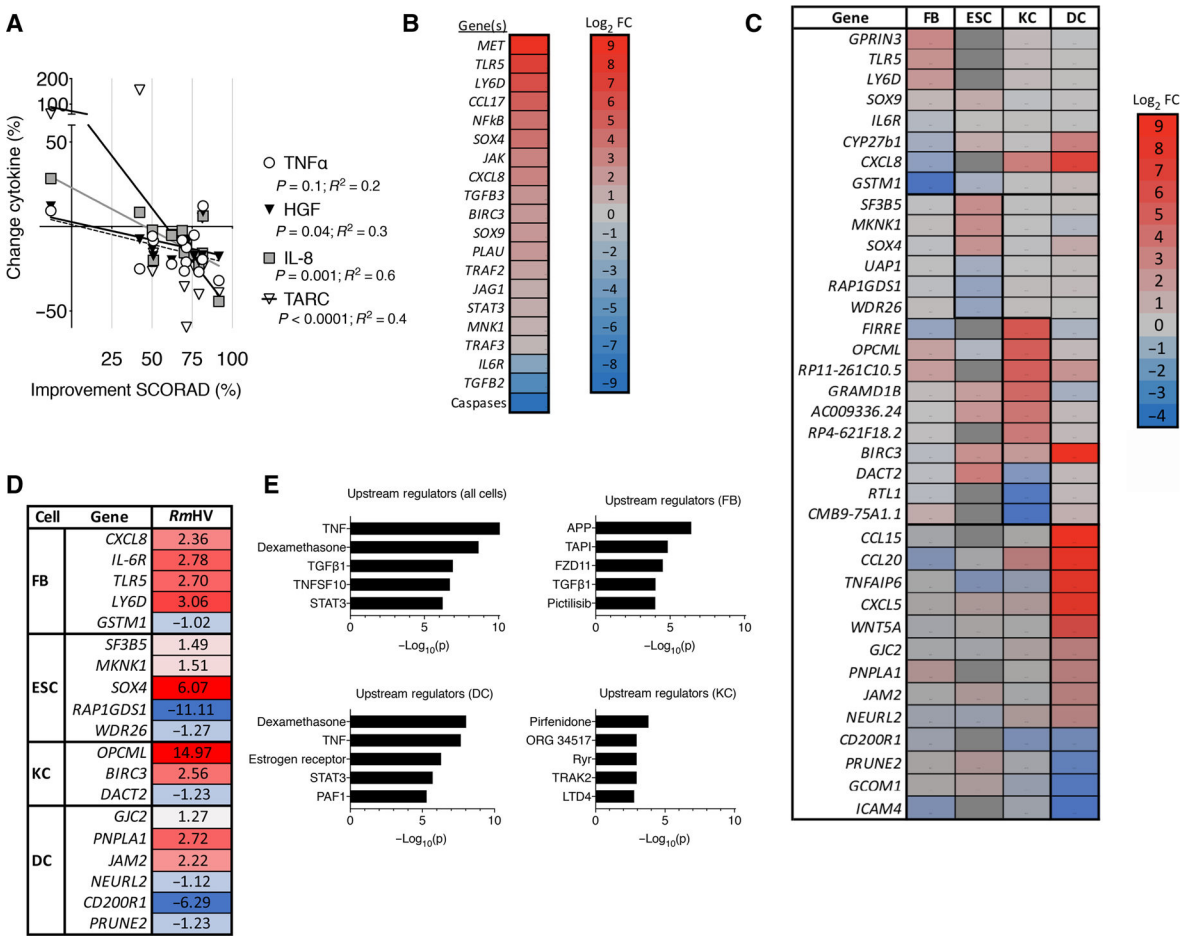

Fig. 4. *R. mucosa* from healthy volunteers activates epithelial cell migration and proliferation.

(**A**) Percent change measured by multiplex ELISA in serum concentrations of TNFα, IL-8, HGF, and TARC before *R. mucosa* treatment (week 0) versus clinical improvement in SCORAD values at week 16 ($n = 14$). (**B**) Heatmap indicates $\log_2$ fold change (Log_2 FC) in RNA sequencing (RNA-seq) transcript abundance for molecular targets and pathways indicated by Ingenuity Pathway Analysis for primary human epithelial cell cultures after 24 hours of stimulation with *Rm*HV or *Rm*AD. (**C**) Heatmap indicates $\log_2$ fold change in RNA-seq transcript abundance in primary human cell cultures of keratinocytes (KC), fibroblasts (FB), dendritic cells (DC), and epithelial follicle stem cells (ESC) stimulated for 24 hours with *Rm*HV or *Rm*AD. Color of target indicates greater (red) or lesser (blue) RNA-seq transcript abundance after *Rm*HV compared to *Rm*AD stimulation. Red/positive numbers indicate up-regulation of transcripts after *Rm*HV versus *Rm*AD stimulation; blue indicates down-regulation except for epithelial follicle stem cells, which was compared to diluent control; dark gray blocks indicate transcripts that were not assessed. (**D**) RTqPCR validation for select transcripts identified by RNA-seq in (C) in two experiments, each with three replicates. (**E**) Upstream regulators determined by Ingenuity Pathway Analysis for indicated cell types and combined cell types assessed after *Rm*HV or *Rm*AD stimulation.

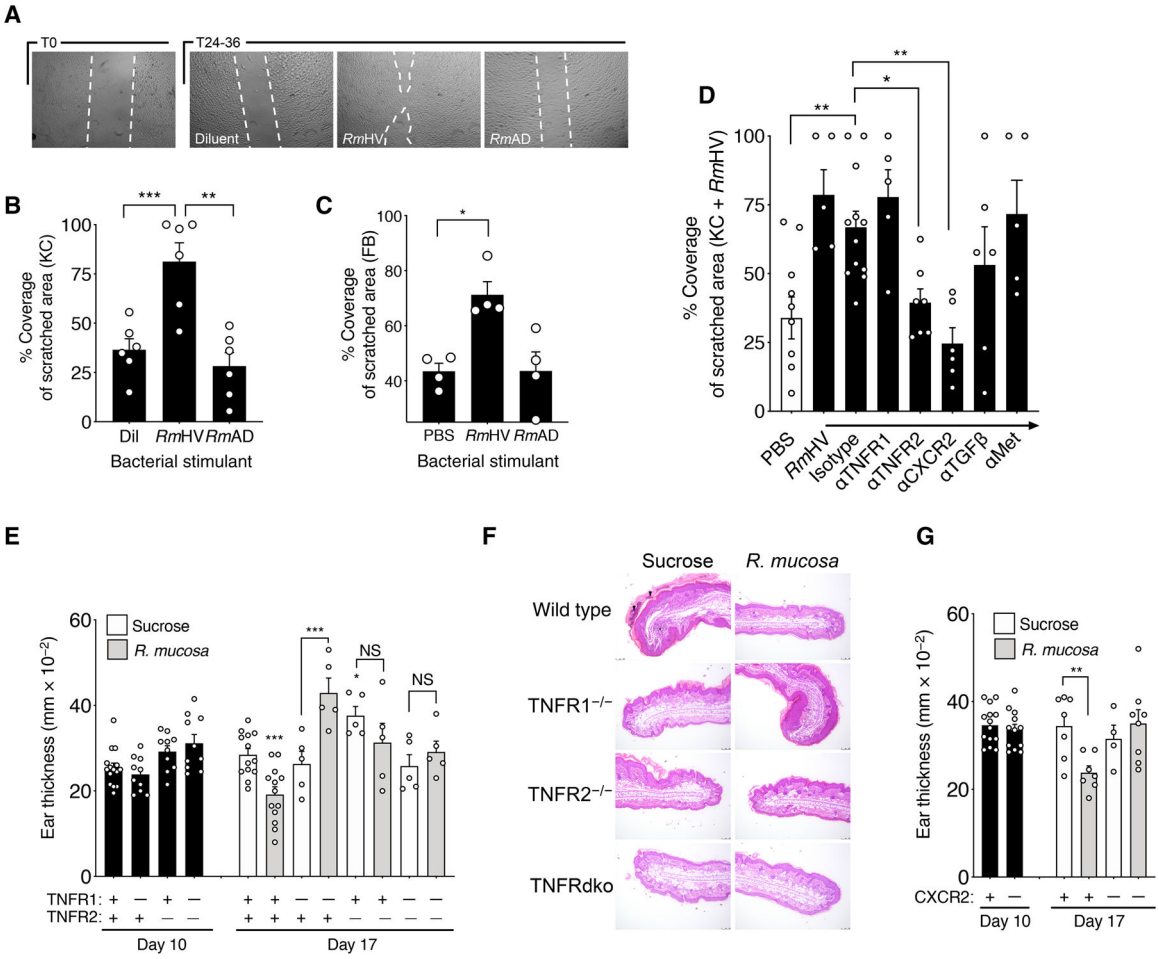

Fig. 5. *R. mucosa* activity was dependent on TNFR signaling.

(**A**) Shown are representative images of the area of cell coverage after a 24- to 36-hour incubation of keratinocytes with *Rm*HV or *Rm*AD in a cellular scratch assay. White dashed lines were digitally added to demarcate scratch borders. (**B** and **C**) Area of coverage for (B) keratinocytes and (C) fibroblasts stimulated with *Rm*HV or *Rm*AD in a 96-well plate. Each experiment was performed with one cell line in replicates indicated by individual dots. PBS, phosphate-buffered saline. (**D**) Keratinocytes pre-treated for 2 hours with antibodies to the indicated receptors or isotype control antibody were stimulated with *Rm*HV or *Rm*AD. (**E**) Mean mouse ear thickness after a 10-day application of MC903 to induce dermatitis (day 10) and after treatment with diluent (sucrose) or *Rm*HV (day 17) for wild-type mice (+) or mice deficient (−) in TNFR1, TNFR2, or both TNF receptors. (**F**) Representative images of mouse ear sections at day 17 after treatment with sucrose diluent control or *Rm*HV stained with hematoxylin and eosin (H&E). Black arrowheads indicate serocellular crusting (inflammatory cells within the layers of thick keratin). Black asterisk indicates inflammatory expansion and infiltration of the underlying dermal stroma. Scale bars, 100 μm. (**G**) Mean mouse ear thickness after application of MC903 and induction of dermatitis (day 10) and after treatment with sucrose diluent control or *Rm*HV (day 17) for wild-type mice (+) or mice deficient (−) in CXCR2. Data are representative of two (E to G) or three or more (A

to D) independent experiments and displayed as the means ± SEM. NS, not significant. *$P <$ 0.05, **$P < 0.01$, and ***$P < 0.001$ determined by paired ANOVA with Dunnett correction.

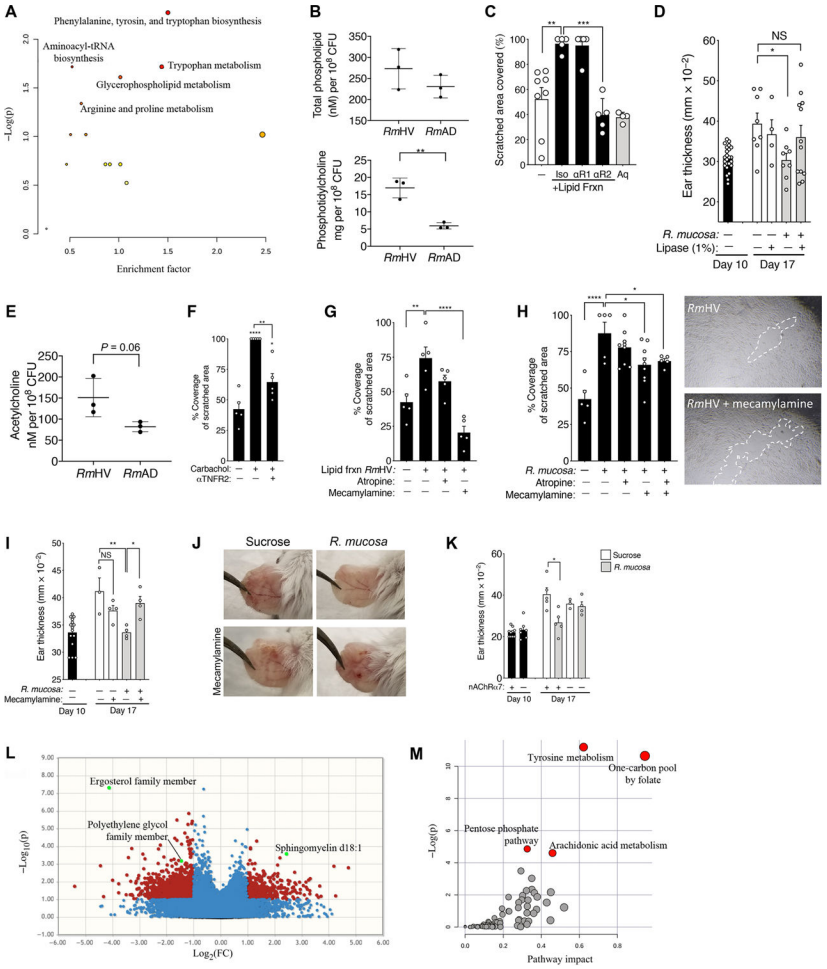

Fig. 6. Lipid mediators of potential *R. mucosa* activity are dependent on cholinergic signaling.

(**A**) Pathway analysis on all annotated features from metabolomics comparison of *Rm*HV and *Rm*AD as determined by MetaboAnalyst. (**B**) Total phospholipid and phosphatidylcholine quantitation by enzymatic assay are presented. tRNA, transfer RNA. (**C**) Shown is coverage area in the cellular scratch assay for fibroblasts treated with an aqueous (Aq) fraction or a lipid fraction extract of *R. mucosa* from healthy volunteers. Fractions were treated with anti-TNFR1 (αR1), anti-TNFR2 (αR2), or isotype control (Iso) antibodies. (**D**) Thickness of mouse ears in the MC903 mouse model treated with *Rm*HV1 or *Rm*HV2 in the presence or absence of 1% lipase from *Candida* spp. (**E**) Production of acetylcholine in response to *Rm*HV and *Rm*AD isolates measured by enzymatic assay. (**F**) Area of coverage for cultured fibroblasts in the cellular scratch assay in the presence or absence of 1 nM carbachol or anti-TNFR2 (αTNFR2) antibody. (**G**) Area of coverage for cultured fibroblasts in the cellular scratch assay treated with lipid fraction extracts of *Rm*HV or *Rm*AD and 5 μM atropine or mecamylamine. (**H**) Mean coverage area for fibroblasts and representative images with digitally added white dashed lines to indicate scratch demarcation after stimulation with *R. mucosa* from healthy volunteers (*Rm*HV) and incubation with 5 μM atropine or mecamylamine. Individual dots represent experimental replicates. (**I** and **J**) Mean mouse ear thickness (I) and representative images (J) for

MC903-treated mice incubated with *R. mucosa* or 5 μM mecamylamine. (**K**) Mean mouse ear thickness after treatment of MC903-treated wild-type or nAChRα7$^{-/-}$ mice (lacking the nicotinic acetylcholine receptor) with *Rm*HV. (**L**) Volcano plot presents metabolite differences in antecubital tape strips taken from patients with AD before and after treatment with *R. mucosa*. Positive $\log_2$ fold change (FC) represents increased detection of a given metabolite in posttreatment samples. Metabolite differences are shown as nonsignificant (blue) or significant by unpaired analysis (red) or paired analysis (green, annotated). (**M**) MetaboAnalyst pathways for all metabolites taken from tape strips showing differences before and after treatment with *R. mucosa*. Data are representative of two (B to H and K) or three or more (I and J) independent experiments and are displayed as the means ± SEM. *$P < 0.05$, **$P < 0.01$, ***$P < 0.001$, and ****$P < 0.0001$ versus enrollment value by paired ANOVA with Dunnett correction.

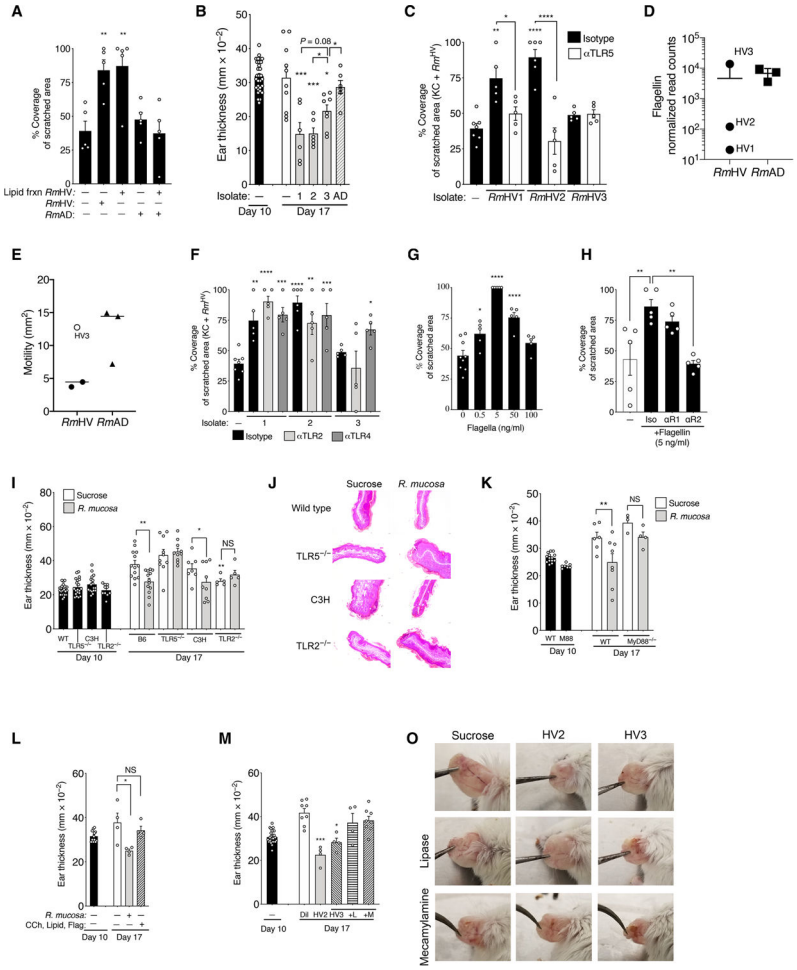

Fig. 7. *R. mucosa* activity depends on TLR5 signaling.

(**A**) Area of coverage for cultured human fibroblasts stimulated with diluent, *Rm*HV1, or *Rm*AD1, with or without addition of the lipid fraction of *Rm*HV1 to *Rm*HV3 in the cellular scratch assay. (**B**) Mean ear thickness for mice treated with *R. mucosa* isolates from *Rm*HV1 to *Rm*HV3 or *Rm*AD is shown. Each dot represents an individual mouse. (**C**) Area of coverage in the cellular scratch assay for human keratinocytes stimulated with *Rm*HV1 to *Rm*HV3 after 2 hours of preincubation with either anti-TLR5 (αTLR5) or isotype control antibody. (**D**) RNA-seq normalized read counts for flagellin expression in *R. mucosa* isolates are depicted. (**E**) Area of growth of *Rm*HV and *Rm*AD in the motility agar assay is shown; open circle indicates *Rm*HV3. (**F**) Area of coverage in the cellular scratch assay for human keratinocytes stimulated with *Rm*HV1 to *Rm*HV3 after 2 hours of preincubation with either anti-TLR2 (αTLR2), anti-TLR4 (αTLR4), or isotype control antibodies. (**G**) Area of coverage is shown for fibroblasts stimulated overnight with recombinant flagellin before scratch induction in the cellular scratch assay. (**H**) Area of coverage is shown for fibroblasts stimulated overnight with recombinant flagellin and anti-TNFR1, anti-TNFR2, or isotype control antibodies in the cellular scratch assay. (**I**) Mean mouse ear thickness in the MC903 mouse model after treatment of wild-type (WT), TLR5$^{-/-}$, TLR4$^{-/-}$ (C3H), or TLR2$^{-/-}$ mice with MC903. Dots represent individual mice. (**J**) Representative H&E-stained

sections of MC903-treated mouse ears from the WT, TLR5$^{-/-}$, TLR4$^{-/-}$ (C3H), or TLR2$^{-/-}$ mice shown in (I). Scale bars, indicate 50 μm. (**K**) Mean mouse ear thickness after treatment of WT or MyD88-deficient (M88; MyD88$^{-/-}$) mice with MC903. (**L**) Shown is mean mouse ear thickness in the MC903 mouse model after treatment of WT mice with either *R. mucosa* or a mixture of 1 nM carbachol (CCh), *Rm*HV lipid extracts (Lipid), or 100 ng per ear of recombinant flagellin (Flag). (**M** to **O**) Mean mouse ear thickness in MC903-treated mice (M) and representative images (O) of mouse ears treated with diluent control (Dil) or *Rm*HV2 or *Rm*HV3 with or without 1% lipase (+L) or 5 μM mecamylamine (+M). Dots represent individual mice (B, I, and K to M) or replicate wells (A, C, and F to H). Data are representative of two (D and E and I to K) or three or more independent experiments and displayed as the means ± SEM. *$P < 0.05$, **$P < 0.01$, ***$P < 0.001$, and ****$P < 0.0001$ versus enrollment value by paired ANOVA with Dunnett correction.

Table 1.

Clinical improvements associated with *R. mucosa* treatment.

Summary of clinical outcomes. SCORAD, EASI, and pruritus values for study participants are shown together with rates of improvement.

SCORAD measures	**Dose escalation *n* = 15**	**10^5 CFU/body site dose *n* = 5**	**Total *n* = 20**
SCORAD50	80.0%	100%	85%
SCORAD75	33.3%	40%	35%
Mean % improvement in SCORAD	64.3%	69.4%	65.6%
EASI measures			
Mean baseline EASI score	7.2	9.5	7.8
Mean week 16 EASI score	1.3	1.8	1.4
Mean % improvement in EASI	75.6%	80.5%	76.8%
EASI50	86.7%	100.0%	90.0%
EASI75	66.7%	80.0%	70.0%
EASI90	40.0%	0.0%	30.0%
Pruritus measures			
Mean baseline pruritus score	6.4	7.1	6.6
Mean week 16 pruritus score	2.3	3.4	2.6
Mean % improvement	59.7%	51.0%	57.6%